Bond-rearrangement and ionization mechanisms in the photo-double-ionization of simple hydrocarbons (C_2H_4, C_2H_3F, and 1,1-$C_2H_2F_2$) near and above threshold

B. Gaire,[1] A. Gatton,[1] F. Wiegandt,[1,2] J. Neff,[1,2] C. Janke,[2] S. Zeller,[2] D. Reedy,[4] J. Rajput,[3] I. Ben-Itzhak,[3] A. L. Landers,[4] A. Belkacem,[1] and Th. Weber[1]

[1]*Chemical Sciences Division, Lawrence Berkeley National Laboratory, Berkeley, California 94720, USA*

[2]*Institut für Kernphysik, Goethe-Universität, Max-von-Laue-Straße 1, Frankfurt am Main 60438, Germany*

[3]*J. R. Macdonald Laboratory, Department of Physics, Kansas State University, Manhattan, Kansas 66506, USA*

[4]*Department of Physics, Auburn University, Alabama 36849, USA*

(Received 19 May 2016; published 14 September 2016)

We investigate bond-rearrangement driven by photo-double-ionization (PDI) near and above the double-ionization threshold in a sequence of carbon-carbon double-bonded hydrocarbon molecules: ethylene, fluoroethylene, and 1,1-difluoroethylene. We employ the kinematically complete cold target recoil ion momentum spectroscopy method to resolve all photo-double-ionization events leading to two-ion fragments. We observe changes in the branching ratios of different dissociative ionization channels depending on the presence of no, one, or two fluorine atoms. The role of the fluorine atom in the bond-rearrangement channels is intriguing, as evident by the reordering of the threshold energies of the PDI in the fluorinated molecules. These effects offer a compelling argument that the electronegativity of the fluorine (or the polarity of the molecule) strongly influences the potential energy surfaces of the molecules and drives bond rearrangement during the dissociation process. The energy sharing and the relative angle between the three-dimensional momentum vectors of the two electrons enable us to distinguish between knockout and other ionization mechanisms of the PDI processes.

DOI: 10.1103/PhysRevA.94.033412

I. INTRODUCTION

Photo-double-ionization (PDI) is a process in which the absorption of a single photon leads to the correlated ejection of two electrons from an atom or molecule. In the PDI of polyatomic molecules multiple competing channels are possible that differ from each other in the type of bond cleavage. The branching ratio of these channels hence shows the likelihood of breaking a particular bond. In many cases bond rearrangement with particle migration occurs in addition or competition to the spontaneous-bond-breaking process. In our previous investigations of the PDI of polyatomic molecules with carbon-carbon double and triple bonds, we have observed predominantly bond-rearrangement channels involving the migration of lighter atoms (for example, H atoms in C_2H_4 and C_2H_2 in Ref. [1]). In the PDI of 1,1-difluoroethylene, where two of the hydrogen atoms of an ethylene molecule are replaced by fluorine atoms, the bond-rearrangement channels involve the migration of both lighter and heavier mass fragments (namely, H and F atoms) [2]. One of the surprising observations is that the molecular hydrogen ion (H_2^+) elimination channel yield is reduced significantly in the PDI of 1,1-$C_2H_2F_2$ (below 1%) compared to the PDI of C_2H_4 (about 7%). This interesting effect motivated us to further explore the bond-rearrangement channels in fluorinated ethylene. In this work we explore the PDI of fluoroethylene (C_2H_3F, also known as vinyl fluoride) in which only one hydrogen atom of an ethylene molecule is replaced by a fluorine atom. This molecule (HH>C=C<HF) can be thought of as an intermediate species between ethylene (HH>C=C<HH) and 1,1-difluoroethylene (HH>C=C<FF) and hence represents a good candidate to investigate the effects of fluorination in hydrocarbons upon photodissociation. One would expect different branching ratios of all the two-ion fragmentation channels due to the presence of no, one, or two fluorine atoms.

The PDI can occur as a direct or indirect ionization process [3,4]. In direct PDI two electrons are simultaneously emitted, without an intermediate step. At least two different mechanisms are plausible. (A) The photon is absorbed by one electron, which kicks out the second electron from the target. This is also known as knockout, or the two-step-one process [5]. (B) The absorption of one photon may lead to a sudden removal of the primary electron. This causes a change in the binding field so that the secondary electron instantaneously relaxes with a certain probability to an unbound state of the remaining ion leaving a doubly charged ion behind. This is known as shake-off process [6,7]. Near the PDI threshold (excess energy below 30 eV) the knock-out mechanisms dominates the shake-off process most of the time. In this energy regime, the signature of the knock-out mechanism is a rather symmetric electron energy distribution and an almost back-to-back emission pattern between the two expelled electrons while a shakeoff electron often has low energy and is emitted more isotropically with respect to the fast electron. In indirect ionization, one inner-shell electron is ionized by the incident photon; the inner-shell vacancy is then filled by an inner- (or outer-) shell electron. The excess energy between the state of the ionized electron and the state of the electron filling the hole is used to release another electron to the continuum. This is generally known as Auger decay. If the first step involves a resonant excitation to a state below or above the single-ionization continuum we call this autoionization [8]. In both Auger decay and autoionization the angular distribution of the second electron does not show a favored back-to-back emission with respect to the photoelectron [2] as it is emitted after the photoelectron is released and hence electron-electron repulsion is negligible. For these indirect-ionization processes angular correlations between both electrons are only mediated via an alignment or orientation of the excited orbital or

superposition of orbitals of the intermediate singly charged molecule (see, e.g., [9]). The occurrence and dominance of direct and indirect PDI can be different for a specific atom [3,10,11] or molecule [12] and it highly depends on the photon energy and target complexity, i.e., the total number of electrons, the available states for relaxation, etc.

In our recent differential studies on the PDI of complex molecules [1,2], we have found that the knockout process of the direct ionization is dominant when the photon energy is near the double-ionization potential of hydrocarbon molecules such as C_2H_4 and $C_2H_2F_2$. This is different from some atomic targets, where shakeoff and/or indirect ionization contributes [13] and even dominates in some cases [14,15]. Likewise for certain molecules, where direct ionization plays a negligible role at the double-ionization threshold, superexcited neutral states, intermediate excited cations, and/or autoionization of atomic fragments in the molecular dissociation drive the indirect-ionization processes in molecules such as O_2, CO, NO, H_2O, and H_2S [12,16,17]. In this work we explore the role of the knockout mechanism in the PDI of C_2H_3F near and above the PDI threshold. The PDI thresholds of the hydrocarbon molecules C_2H_4, C_2H_3F, and $C_2H_2F_2$ under investigation here are roughly the same, i.e., they reside around 29–30 eV.

II. EXPERIMENTAL METHOD

We have used the cold target recoil ion momentum spectroscopy (COLTRIMS) method [18–20] for the coincident detection of two ions and two electrons emerging from the PDI of a single fluoroethylene molecule. Linearly polarized soft-x-ray photons are provided from beamline 10.0.1 of the Advanced Light Source at the Lawrence Berkeley National Laboratory. This photon beam crosses a supersonic jet of fluoroethylene molecules at the interaction region within our three-dimensional (3D) momentum imaging spectrometer. The electrons and ions generated by the photoionization are guided to opposite arms of the spectrometer and detected using multihit capable time- and position-sensitive microchannel plate detectors with delay-line readout [21].

The data are recorded in list mode, i.e., on a shot-by-shot basis, and an intricate offline analysis is performed after the experiment by reading, sorting, and processing the data set under different software conditions. For the PDI with subsequent ionic two-body breakup, 3D momentum vectors of two electrons and two ions are retrieved from the recorded time-of-flight (TOF) and position information utilizing the full strength of our COLTRIMS method. We discuss our findings in the next section.

III. RESULTS AND DISCUSSION

The following five dissociative ionization channels resulting in two-ion fragments are observed in our measurements of PDI of fluoroethylene (C_2H_3F) at photon energies of 40.5 and 55.5 eV (linear polarized light):

$$\begin{aligned} C_2H_3F + E_\gamma &\rightarrow CH_3^+ + CF^+ + 2e^- \\ &\rightarrow CH_2^+ + CHF^+ + 2e^- \\ &\rightarrow H^+ + C_2H_2F^+ + 2e^- \\ &\rightarrow HF^+ + C_2H_2^+ + 2e^- \\ &\rightarrow H_2^+ + C_2HF^+ + 2e^-, \end{aligned}$$

where E_γ represents the photon energy. These channels can be identified as curved diagonal stripes in the raw spectra shown in Fig. 1 for the PDI of C_2H_3F using a photon energy of 40.5 eV. In this figure we plot the yield as a function of the TOF of the first and second ions detected with our apparatus. This is known as a photoion-photoion coincidence (PIPICO) spectrum. Individual channels are analyzed in detail by assigning the mass, charge, TOF, and position on the detector of the respective fragment ions. The kinetic energy of the ions and electrons are obtained from the measured momentum vectors of the individual particles.

Figure 1(b) highlights that for complex polyatomic molecules such as hydrocarbons the fragment mass identification based on the PIPICO alone is not always possible. For example, in the PDI of C_2H_3F the breakup channels $CH_3^+ + CF^+$ and $CH_2^+ + CHF^+$ resulting from a C=C bond cleavage with and without H migration overlap in the PIPICO spectrum. For those cases the position of impact on the detector has to be used for mass analysis in addition to the time-of-flight information. To do so we calculate the momenta

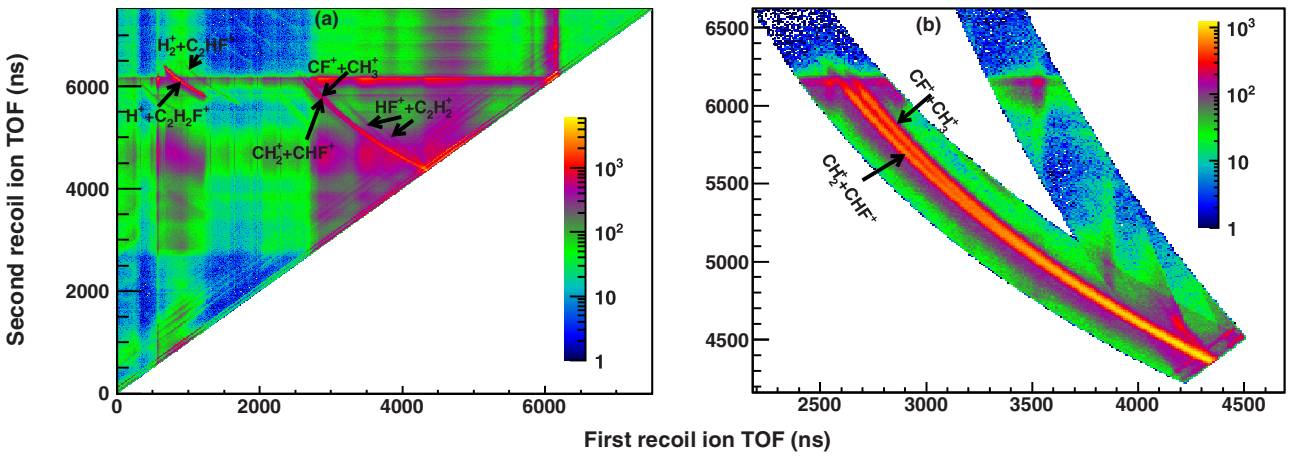

FIG. 1. (a) Photoion-photoion coincidence spectrum, used to identify and separate the different breakup channels resulting from the PDI of C_2H_3F by single photons of 40.5 eV energy. (b) Overlap of the two breakup channels $CH_3^+ + CF^+$ and $CH_2^+ + CHF^+$, which poses a challenge in assigning the correct events (see the text).

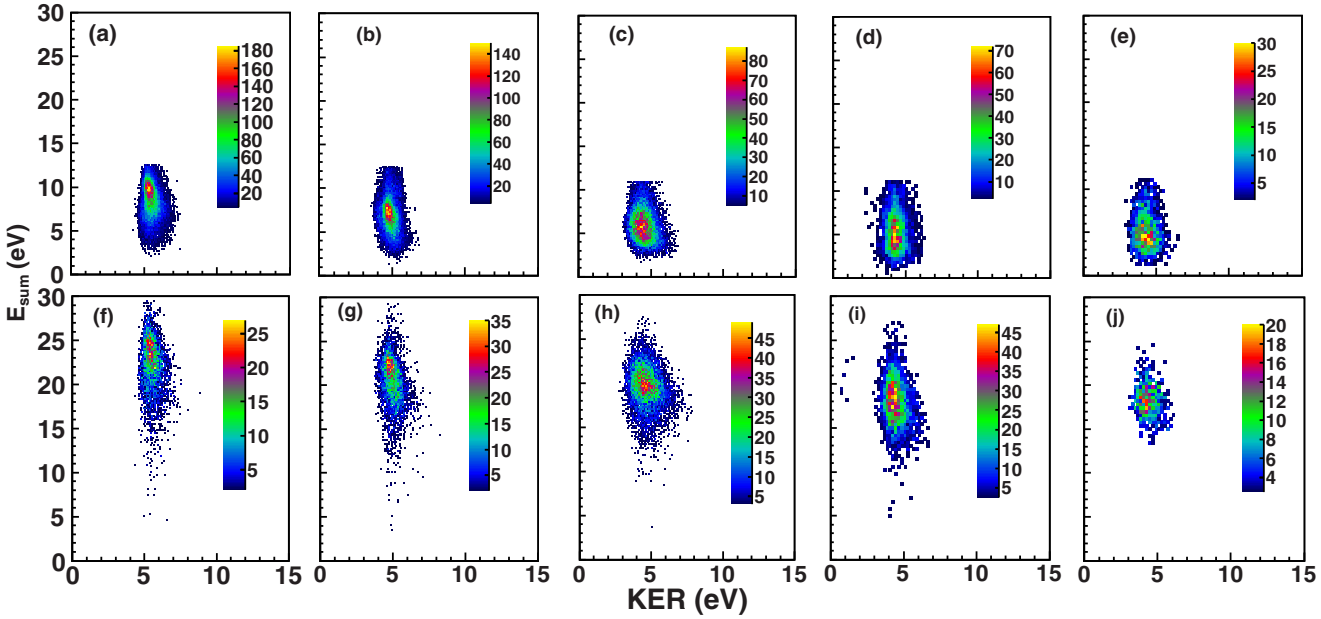

FIG. 2. Electron-ion energy maps shown as a density plot of the breakup yield as a function of the sum of the kinetic energies of the two electrons E_{sum} and the KER of the ions for the DI channels (a) and (f) $CF^+ + CH_3{}^+$, (b) and (g) $CH_2{}^+ + CHF^+$, (c) and (h) $H^+ + C_2H_2F^+$, (d) and (i) $HF^+ + C_2H_2{}^+$, and (e) and (j) $H_2{}^+ + C_2HF^+$ from the PDI of C_2H_3F by linearly polarized light using photon energies of (a)–(e) 40.5 eV and (f)–(j) 55.5 eV.

of each particle for all the possible mass combinations and then check which of the mass assignments results in momenta that better fulfill momentum conservation. Moreover, while the ion pairs overlap in the PIPICO spectrum, the fragment pairs can still be discerned by their difference momenta and their respective angles in space. In our case we choose the molecular orientation along the TOF axis and the kinetic energy release (KER), which comprise all 3D components, i.e., the x and y positions and the TOF of each individual fragment. If the mass assignment is correct the KER is the same for all molecular orientations (not shown here). If this is not the case the fragment energy of the Coulomb explosion is calculated with the wrong mass assignment leading to an incorrect KER and these events need to be discarded. This is done by setting an upper and lower limit for the ion momenta of the lighter fragment of the two possible breakup channels.

A. Energy maps and threshold energies

In the PDI processes studied here the total available energy is distributed between the ejected electrons (we denote the sum of their kinetic energy by E_{sum}), the kinetic energy release of the ions, and possible internal (electronic, vibrational, or rotational) excitations of the molecular ion fragments. Evidently plotting E_{sum} versus the KER is a powerful tool to learn about the relevant potential energy surfaces (PESs) of the intermediate doubly ionized species (see our study on C_2H_4 in Ref. [1]).

The energy maps for the two-ion fragment channels of the PDI of C_2H_3F for photon energies of 40.5 and 55.5 eV are shown in Fig. 2. The peak values of the KER and E_{sum} distributions are also presented in Table I. The differences due to the two photon energies as well as the fragment channels are rather small. There are no obvious secondary islands in the 2D density plots shown in Fig. 2 as found, for instance, in the PDI of C_2H_4 [1]. When surveying the peaks of the KER distributions one can see that their values remain about the same for a given channel at both photon energies. The peak values of the E_{sum} distributions for the two different photon energies increase slightly less than the photon energy (15 eV). This shows that higher-lying intermediate electronic states are populated at higher photon energy. To learn more

TABLE I. Sum of the kinetic energies of the electrons (E_{sum}), kinetic energy release (KER) of the ions (peak positions) and branching ratio (BR) for different ionic two-ion fragmentation channels from the PDI of C_2H_3F using single photons with energies E_γ of 40.5 and 55.5 eV (linearly polarized).

	$E_\gamma = 40.5$ eV			$E_\gamma = 55.5$ eV		
Channel	E_{sum}(eV)	KER (eV)	BR (%)	E_{sum}(eV)	KER (eV)	BR (%)
$CF^+ + CH_3{}^+$	9	5.3	31.8 ± 3.3	21.5	5.4	17.7 ± 2.9
$CH_2{}^+ + CHF^+$	7	4.9	27.8 ± 2.9	20.5	4.9	20.6 ± 3.4
$H^+ + C_2H_2F^+$	6	4.5	32.7 ± 3.3	20	4.5	45.9 ± 7.4
$HF^+ + C_2H_2{}^+$	5	4.2	5.2 ± 0.6	18	4.2	12.1 ± 2.1
$H_2{}^+ + C_2HF^+$	5	4.2	2.4 ± 0.3	18	4.2	3.6 ± 0.7

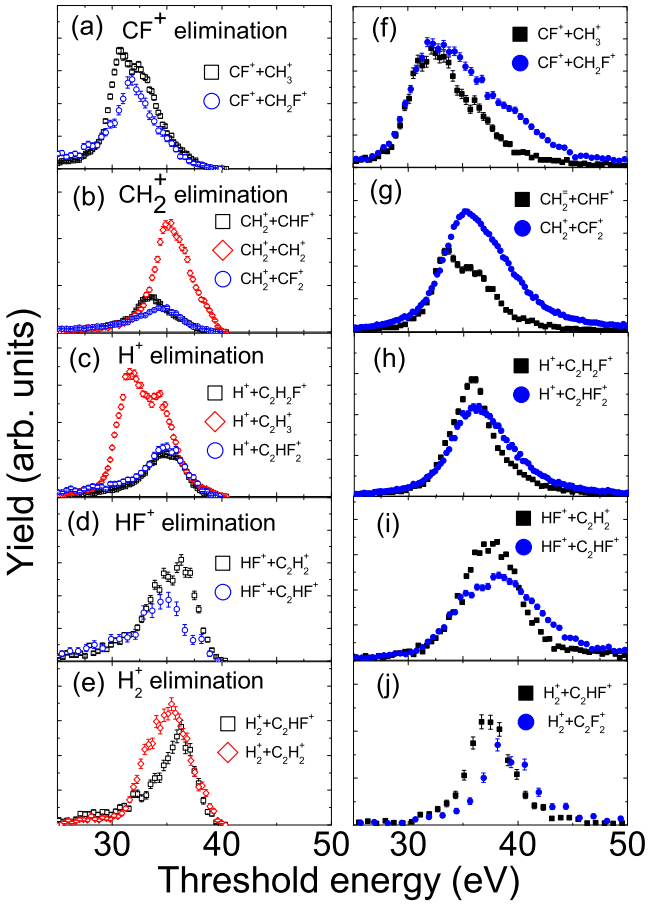

FIG. 3. Threshold energies for the different two-ion breakup channels in the PDI of C_2H_3F using photon energies of (a)–(e) 40.5 eV (black open squares) and (f)–(j) 55.5 eV (black closed squares). The error bars indicate the statistical uncertainty in the data. The data are scaled such that the distributions overlap at either the lower or the higher threshold energy (note that the actual branching ratio is presented in Fig. 6 and Table I). For comparison we have included the data of the PDI of (b), (c), and (e) C_2H_4 (red open diamonds) and (a)–(d) 1,1-$C_2H_2F_2$ for 40 eV photon energy (blue open circles) and (f)–(j) 1,1-$C_2H_2F_2$ for 60 eV photon energy (blue closed circles).

about the electronic states of the fragment ion we calculate the asymptotic energy $E_a = E_\gamma - E_{\rm sum} - {\rm KER}$ for each event, where we call $E_\gamma - E_{\rm sum}$ the threshold energy (see Fig. 3). With increasing photon energy these spectra differ on their falling edge, which confirms that a simultaneous electronic excitation takes place. In these spectra one can identify several peaks in the threshold energies. The trend for the various two-ion fragmentation channels of the PDI of C_2H_3F is very similar to the one observed in the PDI of 1,1-$C_2H_2F_2$ [2] (which is plotted here for comparison). In addition, we also present the threshold energies of the PDI of C_2H_4 in Figs. 3(a)–3(e).

In the case of the PDI of C_2H_4 and 1,1-$C_2H_2F_2$ the nondissociative ionization channel (i.e., the channel resulting in a metastable dication) has the lowest threshold energy [1,2]. For the PDI of C_2H_4 the deprotonation channel has the lowest threshold energy among the dissociative ionization (DI) channels, as one can see in Figs. 3(b), 3(c), and 3(e) (red open diamonds). However, this situation is different in the PDI of 1,1-$C_2H_2F_2$, where the C=C bond breaking with particle migration has the lowest threshold energy (among the DI channels). The presence of the fluorine atoms polarizes the molecule, which is evident in a higher charge of the carbon atom close to that of fluorine [22]. This subsequently results in a weaker C=C bond and hence reduces the threshold energy for the C=C bond cleavage channels. The PDI sequence is continued by the deprotonation channel and the C=C bond breaking without particle migration. The latter two channels have about the same threshold energy. In the case of the PDI of fluoroethylene (C_2H_3F) the trend is yet different again. As one can see from Fig. 3, the C=C bond breaking with hydrogen migration has a lower threshold energy than the C=C bond breaking without particle migration and additionally has two peaks in the energy distribution [see Fig. 3(a), black open squares]. Moreover, the spontaneous C=C bond cleavage channel without particle migration has a lower threshold than the deprotonation channel. The threshold energy distribution of the deprotonation channel (H^+ elimination) in the PDI of C_2H_4 has two peaks, as shown in Fig. 3(c) (red open diamonds). Only the higher threshold energy, part of this distribution overlaps with the threshold energy of the deprotonation channels in the PDI of C_2H_3F (black open squares) and 1,1-$C_2H_2F_2$ (blue open circles), as shown in Fig. 3(c).

The threshold energy of the HF^+ elimination channel in the PDI of both C_2H_3F and 1,1-$C_2H_2F_2$ is about the same [see Fig. 3(d)]. There are at least two different states involved in the PDI of C_2H_3F (black open squares), while the contribution from the higher-lying states (around a threshold energy of 37 eV) is diminished in the PDI of 1,1-$C_2H_2F_2$ (blue open circles). This can be due to the two possibilities of HF bond rearrangement involving bonding of one H and one F atom at one C atom compared to bonding of one H and one F atom across from the C=C double bond. Only the latter scenario is possible in the PDI of 1,1-$C_2H_2F_2$ (blue open circles).

For the PDI of C_2H_3F, the threshold energy for the H_2^+ elimination channel has a double-peak-like structure similar to that in the HF^+ elimination channel, however, the contribution at the lower threshold energy is quite suppressed [compare Figs. 3(d) and 3(e), black open squares]. It appears that the distribution of the H_2^+ elimination channel in the PDI of C_2H_4 [Fig. 3(e), red open diamonds] resembles the HF^+ elimination in the PDI of C_2H_3F [Fig. 3(d), black open squares] much better. One can speculate that this lack of H_2^+ elimination in the PDI of C_2H_3F contributes to the HF^+ elimination channel. In fact, the sum branching ratio of the HF^+ and H_2^+ elimination channels in the PDI of C_2H_3F is similar to the H_2^+ elimination yield in the PDI of C_2H_4 (for 40.5 eV photon energy).

As apparent in Figs. 3(f)–3(j) (black solid squares), for a photon energy of 55.5 eV one can see small bumps in the long tails of the threshold energy distributions of all channels in the PDI of C_2H_3F. This is an indication that higher-lying electronic states are populated by the PDI of C_2H_3F, as they become more accessible at this higher photon energy. A similar trend has been observed in the PDI of 1,1-$C_2H_2F_2$ [2]. We further explore the PDI process by looking into the energy sharing between the two expelled electrons and the relative angle between their 3D momentum vectors. This information helps us to discern between the ionization mechanisms.

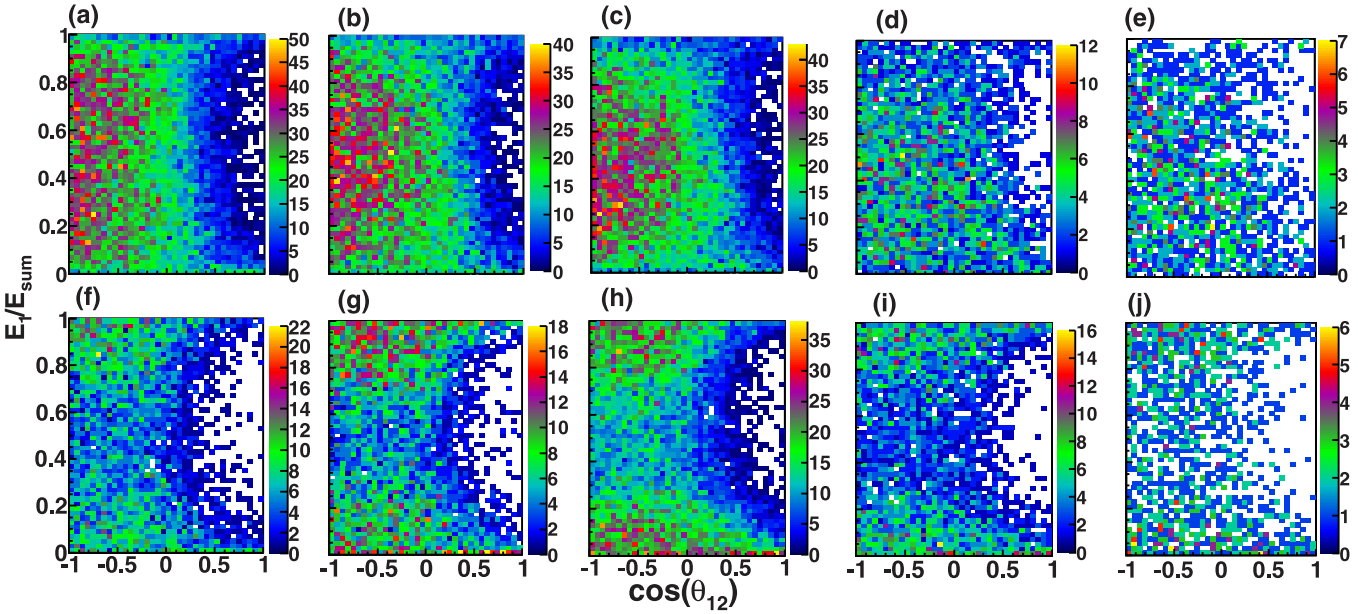

FIG. 4. Electron energy sharing as a function of the cosine of the relative angle θ_{12} between the 3D momentum vectors of the two outgoing electrons for the DI channels: (a) and (f) $CF^+ + CH_3^+$, (b) and (g) $CH_2^+ + CHF^+$, (c) and (h) $H^+ + C_2H_2F^+$, (d) and (i) $HF^+ + C_2H_2^+$, and (e) and (j) $H_2^+ + C_2HF^+$ from the PDI of C_2H_3F using photon energies of (a)–(e) 40.5 eV and (f)–(j) 55.5 eV.

B. Relative energy and angle between electrons

We present, in Fig. 4, the yield as a function of electron energy sharing and relative emission angle θ_{12} for the five different two-ion breakup channels upon PDI by 40.5-eV [Figs. 4(a)–4(e)] and 55.5-eV [Figs. 4(f)–4(j)] photons. At a photon energy of 40.5 eV, the energy sharing is rather uniform and structureless along the $E_1/E_{\rm sum}$ axis [Figs. 4(a)–4(e)]. This is a signature of the knockout mechanism in the direct PDI. However, at a photon energy of 55.5 eV the distribution is different [Figs. 4(f)–4(j)]. There is more yield when one of the electrons has almost all of the excess energy and the second electron is slow, i.e., when $E_1/E_{\rm sum}$ is unequal (i.e., $E_1/E_{\rm sum} < 0.2$ or $E_1/E_{\rm sum} > 0.8$). For this excess energy this is the signature of a shakeoff or indirect PDI process and we cannot clearly disentangle the two possebilites.

For the lower photon energy, the distribution has a higher yield for $\cos(\theta_{12}) = -1$ as shown in Fig. 5, where θ_{12} is the relative angle between the two 3D momentum vectors of the outgoing electrons. We note that in our measurements multihit dead-time problems of the electron detector affect the detection yield of electrons that are emitted in the same direction with similar kinetic energies and hence result in a loss of events at $\cos(\theta_{12}) \approx 1$. The loss of such events depends on the trajectories of the electrons in our 3D momentum spectrometer. We estimate this loss to be up to 30% for $E_1/E_{\rm sum}$ around 1 and about 10% for $E_1/E_{\rm sum}$ around 0. However, the spectra in Figs. 4 and 5 indicate that the electrons are mostly ejected in opposite hemispheres as expected from a two-step-one knockout process [2,23,24]. For the higher photon energy the relative electron emission pattern becomes more uniform as shown in Fig. 5 (solid cirlces). Such a distribution is rather expected for a two-step process like the indirect ionization where both electrons are emitted independently from each other. However, we do not find it to be fully isotropic here. We hence conclude that the PDI of C_2H_3F near the double-ionization threshold is dominated by the knockout mechanism

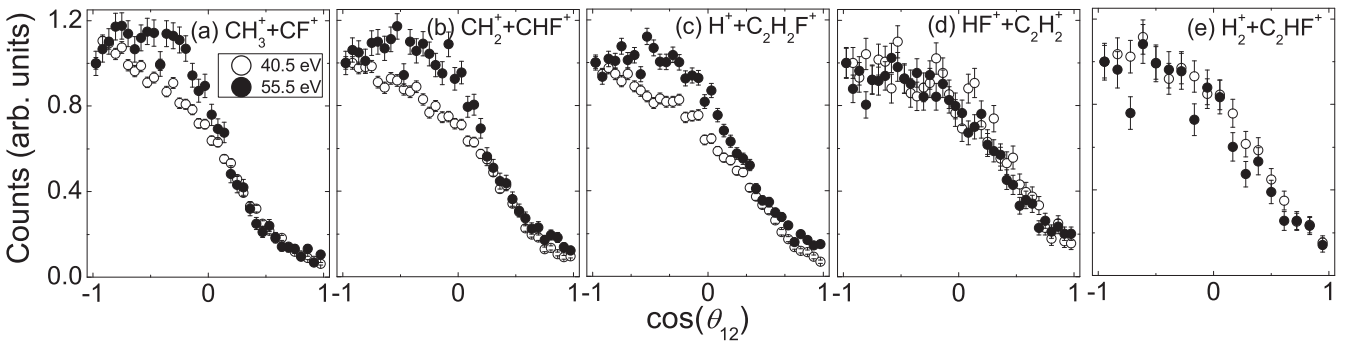

FIG. 5. (a)–(e) Yield as a function of the cosine of the relative emission angle θ_{12} of the two ejected electrons of the PDI of C_2H_3F for the five observed two-body breakup channels as indicated in the spectra. The distributions are normalized to a yield of 1 for $\cos(\theta_{12}) = -1$ for better comparison. The open circles reflect a photon energy of 40.5 eV and the closed circles represent a photon energy of 55.5 eV.

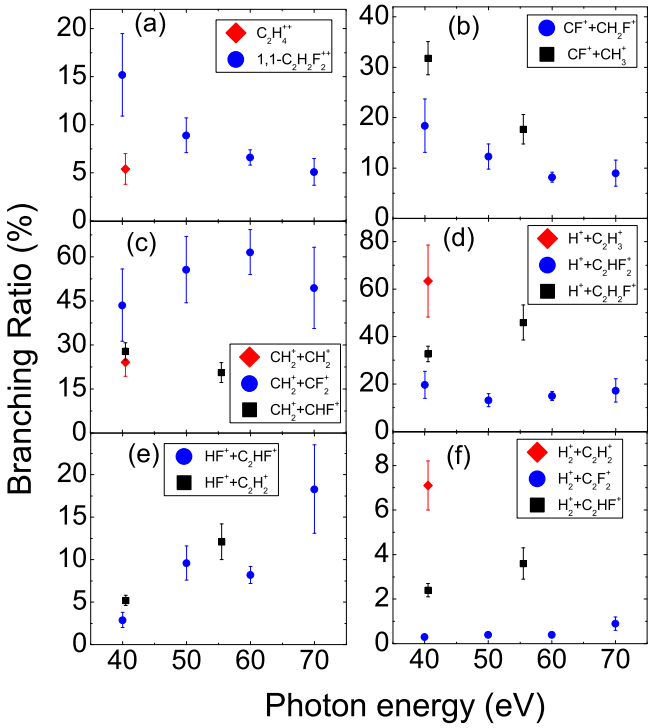

FIG. 6. Branching ratio (in %) of the PDI of C_2H_4 (red closed diamonds), C_2H_3F (black closed squares), and 1,1-$C_2H_2F_2$ (blue closed circles) for a photon energy range of 40–70 eV. The C_2H_4 and 1,1-$C_2H_2F_2$ data are taken from Refs. [1,2], respectively.

of the direct-ionization processes and above the threshold we find fast increasing contributions from shakeoff and/or indirect processes. This fast switching in mechanisms has been also observed in the PDI of 1,1-$C_2H_2F_2$ [2].

C. Branching ratio

The expected variations in the branching ratios of the PDI channels for the different molecules are associated with the nature of the PES of the molecular dication. However, such calculated PESs (or their projections on, or cuts along, some of the many possible degrees of freedom of the polyatomic molecules) for the PDI of C_2H_3F and 1,1-$C_2H_2F_2$ are not available yet. Here we present the branching ratio of the dissociative ionization channels in the PDI of C_2H_3F together with the peak values of the sum of the kinetic energies of the electrons E_{sum} and the KER of the recoiling ions in Table I and in Fig. 6. For a photon energy of 40.5 eV the yields of the deprotonation channel ($H^+ + C_2H_2F^+$) and the C=C bond breaking involving H migration ($CH_3^+ + CF^+$) are very similar (about 32%). A little less likely (about 28%) but within our statistical error bars is the C=C bond cleavage channel without particle migration ($CH_2^+ + CHF^+$). The breakup channel $HF^+ + C_2H_2^+$, which involves an HF bond formation and hence requires F and/or H migration, has a smaller branching ratio of about 5%. This is still (by a factor of 2) more likely than the molecular hydrogen ion (H_2^+) elimination channel ($H_2^+ + C_2HF^+$), which has the lowest yield of about 2.5%.

The trend is different for the photon energy of 55.5 eV. The yields of the C=C bond cleavage channels with and without H migration (i.e., $CH_3^+ + CF^+$ and $CH_2^+ + CHF^+$) have decreased, while the probabilities of the $H^+ + C_2H_2F^+$,$HF^+ + C_2H_2^+$, and $H_2^+ + C_2HF^+$ channels have increased. This scenario is different from the PDI of 1,1-$C_2H_2F_2$ where the C=C cleavage without particle migration was dominant at all photon energies [2]. Obviously the PESs guiding the breakup dynamics must be significantly different. Consequently, we expect this trend to be related to the sum of the kinetic energies of the electrons E_{sum} (shown in the ion-electron energy maps in Fig. 2) or equivalently the threshold energies, defined as the difference between the photon energy and E_{sum} (shown in Fig. 3). As outlined in Sec. III A, the $CH_3^+ + CF^+$ channel has the higher E_{sum} which means that it likely involves the population of a lower-lying electronic state in the dissociation pathway. The ionization cross section to the lower-lying state is higher at the lower photon energy. The other channels have lower E_{sum} (or higher threshold energy) and hence result from the dissociation pathways involving higher-lying excited PESs. The higher-lying states have higher cross sections at the higher photon energy. This is also the reason for the increased yield of the rest of the breakup channels ($H^+ + C_2H_2F^+$,$HF^+ + C_2H_2^+$, and $H_2^+ + C_2HF^+$) at 55.5 eV photon energy.

From the observations above, it is evident that for a systematic and thorough understanding of a particular bond cleavage leading to a specific two-ionic fragment channel, PESs in multiple dimensions are highly desirable. Since we are not aware of any C_2H_3F dicationic PESs in the literature, we interpret the data based on the measurement and compare them to the PDI of C_2H_4 and 1,1-$C_2H_2F_2$. Below we summarize our findings extracted by comparing the PDI of C_2H_4, 1,1-$C_2H_2F_2$, and C_2H_3F. The channels are listed based on their ascending threshold energies.

(i) Metastable dications. Metastable dications are not observed in the PDI of C_2H_3F. The ground-state equilibrium geometry of the C_2H_3F system is planar and belongs to the C_s point group [25]. As pointed out in Ref. [22], the preferred structure of the C_2H_3F dication is a perpendicular geometry while its stability is diminished. It is conceivable that once the dication is formed it immediately dissociates into fragments, hence resulting in a nonstable dication. This situation is different for the PDI of C_2H_4 and 1,1-$C_2H_2F_2$ molecules, where we have observed significant fractions of metastable dications at about 40 eV photon energy [see Fig. 6(a)]. The threshold energies for these metastable dications were the lowest of all the PDI channels [1,2].

(ii) CF^+ elimination. The CF^+ elimination is an intriguing channel since it involves particle migration, C=C bond cleavage, and bond rearrangement. For the PDI of C_2H_3F molecules we have observed this channel for both photon energies used in the present work. It involves hydrogen migration and C=C bond breaking resulting in $CH_3^+ + CF^+$. It is also observed in the PDI of the polar 1,1-$C_2H_2F_2$ molecule leading to the $CH_2F^+ + CF^+$ breakup channel requiring a fluorine migration and a C=C bond breaking [2]. However, the equivalent channel leading to $CH_3^+ + CH^+$ is not observed in the case of the PDI of the nonpolar ethylene molecule in our earlier work [1]. For both polar molecules C_2H_3F and

1,1-$C_2H_2F_2$ the threshold energies for CF^+ elimination is lower than the C=C bond-breaking channel without particle migration. These observations suggest that the substitution of a hydrogen atom with the electronegative fluorine redistributes the charges in the dication and hence deforms the PES such that a new fragmentation channel opens.

For the higher photon energy the yield of the fragmentation channel producing CF+ ions and involving the migration of hydrogen and fluorine goes down for both species C_2H_3F and 1,1-$C_2H_2F_2$ [see Fig. 6(b)]. This is because the threshold energies for these channels are relatively low (see Fig. 3). At higher photon energies the population of the higher-lying electronic states is enhanced, while the population of the lower-lying electronic states is reduced. This causes the yield of this fragmentation channel to die out.

(iii) CH_2^+ elimination. For all three molecules C_2H_4, C_2H_3F, and 1,1-$C_2H_2F_2$ this channel results from the spontaneous breaking of the C=C bond without particle migration upon photo-double-ionization. Comparing the yields of the different species for all photon energies, the yield of this breakup channel is always the highest for 1,1-$C_2H_2F_2$, as shown in Fig. 6(c). It appears that the more asymmetric the masses of the constituent atoms across the C=C bond are, the more likely the C=C bond breaking without particle migration seems to be.

(iv) H^+ elimination. The loss of a proton (H^+) in a molecular fragmentation is often called a deprotonation channel. The presence of more hydrogen atoms in a molecule increases the chances for the production of H^+ fragments from the cleavage of one of the C-H bonds, i.e., a higher yield of deprotonation is expected for the PDI of C_2H_4, as shown in Fig. 6(d) for the photon energies covered in our measurements. However, it seems that for a specific molecule like C_2H_3F or 1,1-$C_2H_2F_2$ the deprotonation yield stays almost flat as a function of the photon energy E_γ(40−70 eV).

At a photon energy of 40 eV, the deprotonation channel is dominant in the PDI of ethylene [see Fig. 6(d)] and is much stronger than in the PDI of C_2H_3F and 1,1-$C_2H_2F_2$. However, this role is reversed in the C=C bond-breaking channel at 40 eV [see Fig. 6(c)] where the CH_2^+ elimination in the PDI of fluoroethylene and difluoroethylene dominates. The yields are also reversed for the PDI of C_2H_3F and 1,1-$C_2H_2F_2$ at a photon energy of 55 eV.

(v) HF^+ elimination. The HF^+ elimination channels depicted in Fig. 6(e) involve particle migration and bond rearrangement without breaking the C=C bond. There are at least two ways to form the HF^+ ion in the case of the PDI of fluoroethylene (C_2H_3F): Either both the H and F atoms from the same side of the C=C bond come together or the H and F atoms from across the C=C bond can come closer and form the HF^+ ion. For the PDI of difluoroethylene (1,1-$C_2H_2F_2$) only the H and F atoms from across the C=C bond can lead to the formation of HF^+. It is conceivable that the probability for an additional and simultaneous migration of another H or F atom during this dissociation process is rather low. Hence, one can expect that the HF^+ fragmentation channel leaves an acetylene-like cation behind, i.e., not a lone C atom on one side. However, we have no experimental proof to support this scenario.

For both molecules C_2H_3F and 1,1-$C_2H_2F_2$ the yield of the HF^+ elimination channel goes up with the photon energy E_γ. The branching ratio more than doubles when the photon energy changes from 40 eV to 55 eV for C_2H_3F and increases in a similar way for the PDI of 1,1-$C_2H_2F_2$ [see Fig. 6(e)].

(vi) H_2^+ elimination. The molecular hydrogen ion H_2^+ elimination channel yield is presented in Fig. 6(f). This channel is another example of a fragmentation channel involving bond rearrangement in the PDI of C_2H_4, C_2H_3F, and 1,1-$C_2H_2F_2$. For C_2H_4 and C_2H_3F it may be accompanied by additional H migration leading to an ethylidinelike (i.e., H_3CCH or H_3CCF) transient state. For the PDI of 1,1-$C_2H_2F_2$ an F atom may travel across the C=C bond; however, we had no experimental means at hand to detect this. For all molecules the yield of this PDI breakup is the lowest of all the two-ion fragment channels. It is only 7% in ethylene, 2.4% in fluoroethylene, and 0.3% in difluoroethylene at a photon energy of around 40 eV. It appears that, for a given photon energy, the yield depends on the number of H atoms in the molecule and hence resembles the pattern of the deprotonation channel [compare Figs. 6(d) and 6(f)].

IV. SUMMARY

We have explored the photo-double-ionization of single fluoroethylene (C_2H_3F) molecules near and above the threshold with single linear polarized photons of 40.5 and 55.5 eV energy. We compared our findings with the PDI of ethylene (C_2H_4) and 1,1-difluoroethylene (1,1-$C_2H_2F_2$) molecules. The energy sharing between the expelled electrons is uniform and structureless for a photon energy close to the double-ionization threshold (e.g., 40 eV). Here the PDI process is dominated by the knockout mechanism. For the higher photon energy (55.5 eV) this mechanisms dies out. At this and higher photon energies higher-lying electronic states are accessible and they change the branching ratios of the molecular fragmentation channels via indirect PDI.

The branching ratios change differently among the dissociative ionization channels of these molecules due to the presence of no, one, or two fluorine atoms. The fluorine atoms polarize the molecules and strongly influence the dissociation dynamics and bond rearrangement as evident by the drastic changes in the threshold energies of comparable two-ion fragmentation channels. To gain more insight into the dissociation pathways the potential energy surfaces of the cation and dication states of these molecules are highly desired and need to be calculated. Our findings may stimulate time-resolved measurements to investigate these fundamental bond-rearrangement processes on their natural (ultrafast) time scales of particle migration using pump-probe schemes.

ACKNOWLEDGMENTS

This research used the Advance Light Source and resources of the National Energy Research Scientific Computing Center, DOE Offices of Science User Facilities supported by the Director, Office of Science, Office of Basic Energy Sciences, the Division of Chemical Sciences, Geosciences, and Biosciences of the U.S. Department of Energy at LBNL under Contract No. DE-AC02-05CH11231. We thank the staff of the Advanced Light Source, in particular beamline 10.0.1 scientists for their outstanding support. JRML personnel were supported by Grant No. DE-FG02-86ER13491 from

the same funding agency. We acknowledge financial support from the Deutsche Akademische Austausch Dienst and the Deutsche Forschungs Gemeinschaft. A.G. acknowledges financial support from the ALS via the Doctoral Fellowship in Residence. We thank Reinhard Dörner for helpful discussions. We are indebted to the RoentDek Company for long-term support with detector software and hardware and to M. Schoeffler and T. Jahnke for continuous development of and assistance with the spectrometer simulations and data analysis.

[1] B. Gaire *et al.*, Phys. Rev. A **89**, 013403 (2014).
[2] B. Gaire, I. Bocharova, F. P. Sturm, N. Gehrken, J. Rist, H. Sann, M. Kunitski, J. Williams, M. S. Schöffler, T. Jahnke, B. Berry, M. Zohrabi, M. Keiling, A. Moradmand, A. L. Landers, A. Belkacem, R. Dörner, I. Ben-Itzhak, and T. Weber, Phys. Rev. A **89**, 043423 (2014).
[3] P. Bolognesi, G. C. King, and L. Avaldi, Rad. Phys. Chem. **70**, 207 (2004).
[4] L. Avaldi and A. Huetz, J. Phys. B **38**, S861 (2005).
[5] T. Ishihara, K. Hino, and J. H. McGuire, Phys. Rev. A **44**, R6980 (1991).
[6] V. Schmidt, N. Sandner, H. Kuntzemueller, P. Dhez, F. Wuilleumier, and E. Kaellne, Phys. Rev. A **13**, 1748 (1976).
[7] T. Schneider, P. Leszek Chocian, and J. M. Rost, Phys. Rev. Lett. **89**, 073002 (2002).
[8] A. Russek, M. R. Patterson, and R. L. Becker, Phys. Rev. **167**, 17 (1968).
[9] M. S. Schöffler *et al.*, Science **320**, 920 (2008).
[10] J. H. D. Eland, O. Vieuxmaire, T. Kinugawa, P. Lablanquie, R. I. Hall, and F. Penent, Phys. Rev. Lett. **90**, 053003 (2003).
[11] M. Boettcher, H. Rottke, N. Zhavoronkov, W. Sandner, P. Agostini, M. Gisselbrecht, and A. Huetz, J. Phys. B **38**, L389 (2005).
[12] S. Hsieh and J. H. D. Eland, J. Phys. B **29**, 5795 (1996).
[13] D. Proulox and R. Shakeshaft, Phys. Rev. A **48**, R875(R) (1993).
[14] J. H. D. Eland and R. Feifel, J. Phys. Chem. A **108**, 9721 (2004).
[15] J. H. D. Eland, J. Electron Spectrosc. Relat. Phenom. **144–147**, 1145 (2005).
[16] R. Feifel, D. Edvardsson, and J. H. D. Eland, J. Chem. Phys. **122**, 144308 (2005).
[17] J. H. D. Eland, P. Lablanquie, M. Lavollee, M. Simon, R. I. Hall, M. Hochlaf, and F. Penent, J. Phys. B **30**, 2177 (1997).
[18] J. Ullrich, R. Moshammer, A. Dorn, R. Dörner, L. P. H. Schmidt, and H. Schmidt-Böcking, Rep. Prog. Phys. **66**, 1463 (2003).
[19] T. Jahnke, T. Weber, T. Osipov, A. L. Landers, O. Jagutzki, L. P. H. Schmidt, C. L. Cocke, M. H. Prior, H. Schmidt-Böcking, and R. Dörner, J. Electron Spectrosc. Relat. Phenom. **141**, 229 (2004).
[20] R. Dörner, V. Mergel, O. Jagutzki, L. Spielberger, J. Ullrich, R. Moshammer, and H. Schmidt-Böcking, Phys. Rep. **330**, 95 (2000).
[21] Details can be found at www.roentdek.com
[22] G. Frenking, W. Koch, and H. Schwarz, J. Comput. Chem., **7**, 406 (1986).
[23] L. Malegat, F. Citrini, P. Selles, and P. Archirel, J. Phys. B **33**, 2409 (2000).
[24] D. P. Secombe, S. A. Collins, T. J. Reddish, P. Selles, L. Malegat, A. K. Kazansky, and A. Huetz, J. Phys. B **35**, 3767 (2002).
[25] M. Barbatti, A. J. A. Aquino, and H. Lischka, J. Phys. Chem. A **109**, 5168 (2005).